Molecular-Scale Hybridization of Clay Monolayers and Conducting Polymer for Thin-Film Supercapacitors

Jingwen Zhao, Simin Xu, Kristina Tschulik, Richard G. Compton, Min Wei, Dermot O'Hare,* David G. Evans, and Xue Duan*

Development of electrode materials with well-defined architectures is a fruitful and profitable approach for achieving highly-efficient energy storage systems. A molecular-scale hybrid system is presented based on the self-assembly of CoNi-layered double hydroxide (CoNi-LDH) monolayers and the conducting polymer (poly(3,4-ethylene dioxythiophene):poly(styrene sulfonate), denoted as PEDOT:PSS) into an alternating-layer superlattice. Owing to the homogeneous interface and intimate interaction, the resulting CoNi-LDH/PEDOT:PSS hybrid materials possess a simultaneous enhancement in ion and charge-carrier transport and exhibit improved capacitive properties with a high specific capacitance (960 F g^{-1} at 2 A g^{-1}) and excellent rate capability (83.7% retention at 30 A g^{-1}). In addition, an in-plane supercapacitor device with an interdigital design is fabricated based on a CoNi-LDH/PEDOT:PSS thin film, delivering a significantly enhanced energy and power output (an energy density of 46.1 Wh kg^{-1} at 11.9 kW kg^{-1}). Its application in miniaturized devices is further demonstrated by successfully driving a photodetector. These characteristics demonstrate that the molecular-scale assembly of LDH monolayers and the conducting polymer is promising for energy storage and conversion applications in miniaturized electronics.

1. Introduction

The continued miniaturization of wearable/portable electronics have made micro-power sources with compact, lightweight, and flexible features a critical prerequisite.[1–3] Of the various power source devices, thin-film supercapacitors (SCs) are considered to be highly competitive candidates that can potentially be integrated on a chip along with the necessary electronic components.[4–6] Although significant advances in ultrahigh power density have been realized for carbon/polymer-based electrode materials, film-type SCs normally suffer from low energy density.[7–12] Therefore, the development of energy storage materials that combine the power density of SCs with the energy density of batteries is significantly crucial to advance portable and distributed power technology.

Great efforts have been devoted to overcoming this limitation by incorporating transition metal compounds as pseudocapacitive species with carbons/conducting polymers and achieving enhanced energy densities.[13–16] Superior to single phase materials, hybrid systems integrate two or more individual constituents with complementary properties for improved capacitive behavior.[17–19] Unfortunately, most approaches rely on fabricating the phase interface at a meso- or nano-scale level; consequently, a large portion of the pseudocapacitive phase (especially that internal to the contact) remains blocked from direct contact with conductive backbones, which inevitably leads to irreversible charge-transfer loss. Taking into account the crucial role of interfaces within an organized hybrid system, if individual components are fully hybridized on a molecular scale, the overall energy storage performance would be further boosted based on a more homogeneous interface distribution and stable charge-carrier transport.

Thus, a primary requirement is undoubtedly the creation of appropriate ultrathin materials with at least one characteristic dimension at the molecular scale.[20,21] Layered double hydroxides (LDHs) belong to a class of brucite-like clays, providing tunable intralayer metal cations and interlayer anions.[22–25] Among their distinctive features, atomic-thin LDH monolayers with an ultimate 2D anisotropy can be obtained based on a liquid exfoliation strategy.[26–28] The electrochemically accessible $M(OH)_6$ (M refers to transitional metal cations) units in the host layers present the promise of attractive redox reactions; however, a high energy density and rate capability are in practice hard to be achieved simultaneously as a consequence of the observed semiconducting or insulating properties.[29–31] On the contrary, conducting polymers facilitate charge transport in the electrochemical process, but suffer from mechanical brittleness and poor cycling stability.[32–35] To solve this conundrum,

Dr. J. Zhao, S. Xu, Prof. M. Wei, Prof. D. G. Evans, Prof. X. Duan
State Key Laboratory of Chemical Resource Engineering
Beijing University of Chemical Technology
Beijing 100029, P. R. China
E-mail: weimin@mail.buct.edu.cn

Dr. K. Tschulik, Prof. R. G. Compton
Physical and Theoretical Chemistry Laboratory
Department of Chemistry
University of Oxford
Oxford OX1 3QZ, UK

Prof. D. O'Hare
Chemistry Research Laboratory
Department of Chemistry
University of Oxford
Oxford OX1 3TA, UK
E-mail: dermot.ohare@chem.ox.ac.uk

DOI: 10.1002/adfm.201500408

hybridizing ultrathin LDH structures with conducting polymers at a molecular level, so as to fully harvest the synergistic effect, could be an effective route to obtain satisfactory overall supercapacitive performance.

Herein, we develop a superlattice heterostructure composed of CoNi-LDH monolayers and a commercial polymer PEDOT:PSS via the electrostatic self-assembly route. The oriented and ordered organic–inorganic assembly with a molecular-scale distribution of individual active species is shown to yield a largely improved capacitance and rate capability. From the structural perspective, an intimate and homogeneous interfacial bonding between the LDH monolayers and the interlayer PEDOT:PSS is essential for superior charge storage properties. The LDH monolayers provide a restricted microenvironment for the accommodation of the conducting polymer with desirable spatial arrangement and doping level; while the PEDOT:PSS molecules serve as a multilayer conductive network to facilitate the charge collection and transport. Moreover, the long-range periodic stacking affords a favorable ionic accessibility to the inner surface of LDH active sites. This molecular-scale design makes a key contribution to the promising overall performance of the thin-film SC device with a compatible in-plane configuration.

2. Results and Discussion

2.1. Morphological and Structural Study on the CoNi-LDH/PEDOT:PSS Assembly

CoNi-LDH monolayers and PEDOT:PSS were incorporated into a self-assembly system, serving as the positively and negatively charged building blocks, respectively (Figures S1,S2, Supporting Information). Based on the charge matching hypothesis (see Supporting Information for details), the CoNi-LDH/PEDOT:PSS hybrid structure was precisely fabricated via an electrostatic interaction, as displayed in **Scheme 1**. Cross-sectional scanning electron microscope (SEM) images (**Figure 1**a,b) show the well-ordered and layer-shaped structure of the resulting LDH/PEDOT:PSS material, from which the observed ripples and corrugations reflect the flexibility. Transmission electron microscopy (TEM) observations with various magnifications also provide direct evidence for the formation of highly organized assembly (Figures 1c–e and S3, Supporting Information). The clear lattice fringes along the *c*-direction (Figure 1e) as well as the corresponding symmetric diffraction spots of the fast Fourier transform (FFT) pattern (Figure 1e, inset) indicate a high-quality superlattice arrangement. A high-resolution TEM (HRTEM) image (Figure 1f) reveals well-resolved light and dark contrast fringes with a different thickness, which can be attributed to alternating PEDOT:PSS molecular layers and LDH monolayers, respectively. The lamellar fringe is not completely parallel but slightly twisted in some areas, suggesting the intrinsic flexibility of the CoNi-LDH/PEDOT:PSS hybrid material.

The XRD pattern (Figure 1g) of the CoNi-LDH/PEDOT:PSS product illustrates multiple Bragg reflections at $2\theta = 4.7°$, 9.4°, 14.2°, and 19.0°, which can be attributed to the so-called superlattice reflections of the repeating inorganic-organic hybrid.[27,29] These Bragg reflections are equally spaced (00*l*) harmonic series with a periodicity of 1.88 nm, demonstrating an extremely good *c*-oriented heterostacking. Allowing for a crystallographic thickness of ≈0.48 nm for a single LDH monolayer,[26] the interlayer height of PEDOT:PSS is evaluated as ≈1.40 nm. No other crystalline phase is detected, indicating the purity of CoNi-LDH/PEDOT:PSS superlattice material. When the PEDOT:PSS concentration decreases in the synthesis process, then a CO_3^{2-}-containing LDH phase, CoNi-LDH is observed in the XRD pattern (Figure S4, Supporting Information). A comparison sample of CoNi-LDH/PSS without PEDOT was also prepared by using the same method, with an estimated repeating distance of 1.47 nm (Figure S5, Supporting Information). A theoretical structural model for CoNi-LDH/PEDOT:PSS is shown in Figure 1h. After 1000 ps of molecular dynamics simulation, the result displays a single-layer arrangement of PEDOT:PSS in the interlayer region of LDH monolayers. The simulated basal spacing along the *c*-axis is 19 Å, which matches well with the XRD observation. Moreover, the binding energy between LDH monolayers and PEDOT:PSS is calculated to be 0.64 eV per EDOT, which is mainly composed of hydrogen bonding and coulomb forces (Figure S6, Supporting Information). The high-angle annular dark-field scanning transmission electron microscopy (HAADF-STEM) image of CoNi-LDH/PEDOT:PSS (**Figure 2**a) also exhibits the typical layered morphology. Elemental mapping profiles (Figure 2b–d) correspond to the K-edge signals of Co, Ni, and S, respectively, in which a uniform elemental distribution is observed. This validates the intimate assembling of LDH monolayers and PEDOT:PSS, which is further endorsed by SEM EDS results (Figure S7, Supporting Information).

The in-plane TEM image (*ab*-plane) of CoNi-LDH/PEDOT:PSS displays the PEDOT:PSS immobilized in the LDH interlayer with an expanded-coiled/linear conformation (**Figure 3**a), rather different from the coiled morphology of pristine PEDOT:PSS (Figure S2, Supporting Information). This verifies that the confined gallery of LDH

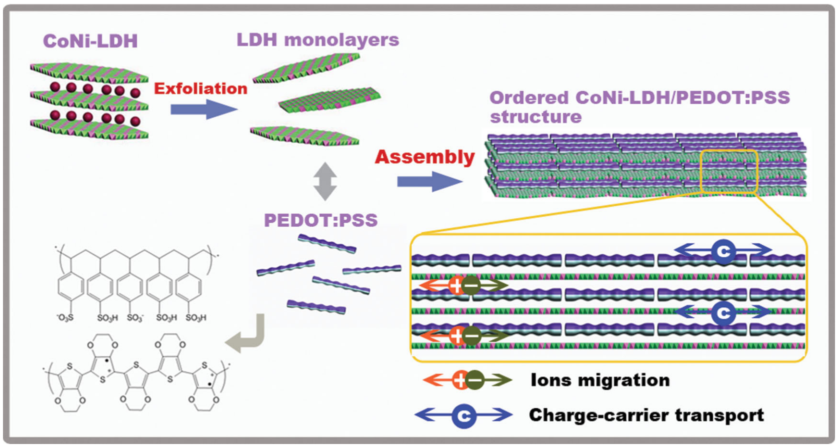

Scheme 1. Schematic illustration for the assembly of CoNi-LDH monolayers and PEDOT:PSS.

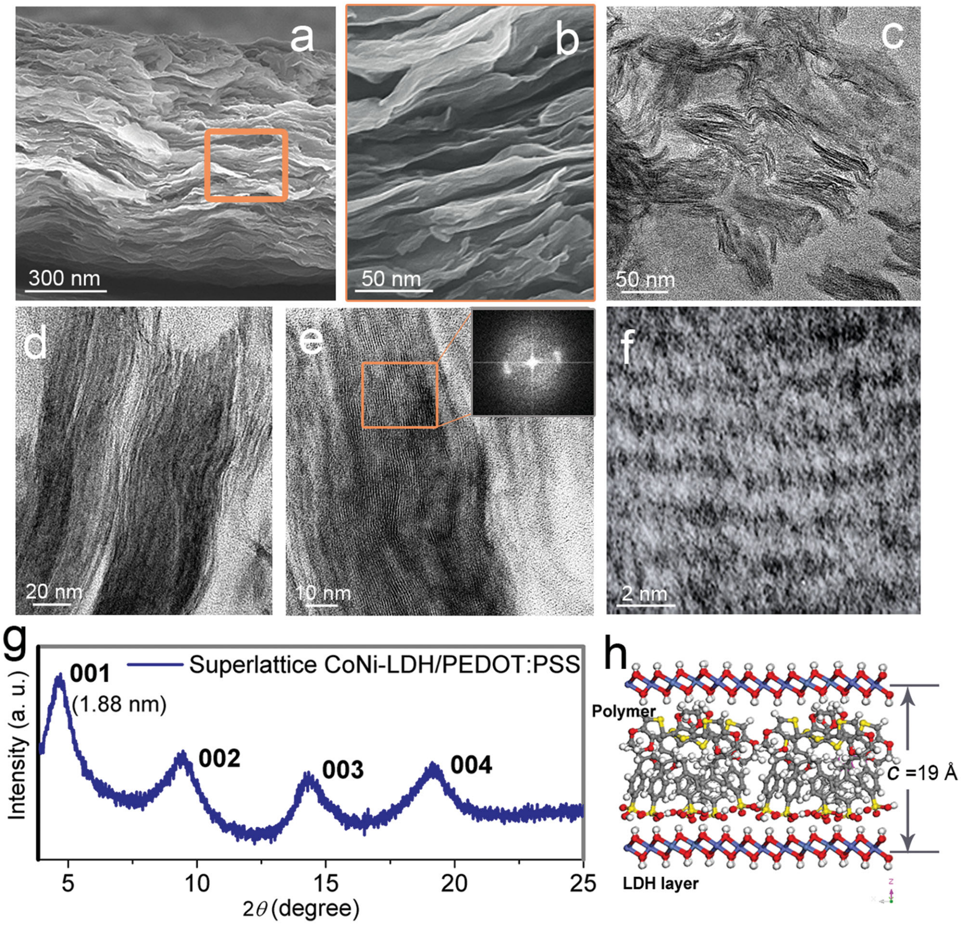

Figure 1. a,b) Cross-sectional SEM, c–e) TEM images, and f) HRTEM image of the CoNi-LDH/PEDOT:PSS; g) XRD pattern of the CoNi-LDH/PEDOT:PSS superlattice structure; h) side-view of the CoNi-LDH/PEDOT:PSS structure model.

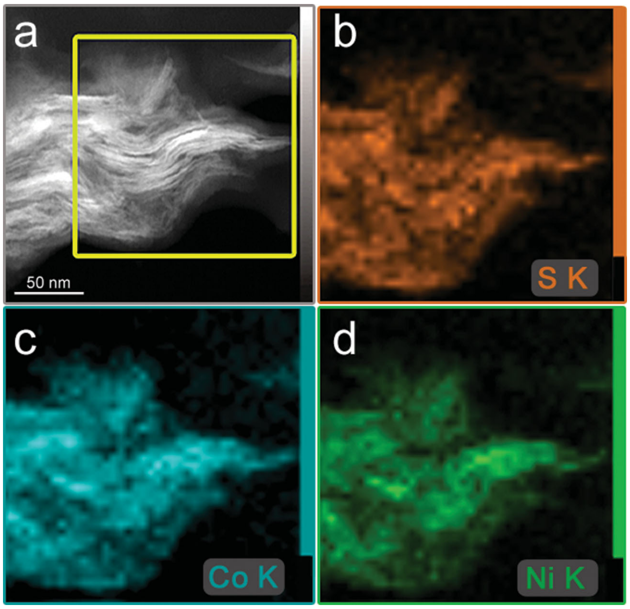

Figure 2. a) Cross-sectional HADDF-STEM image and EDS mapping of the elements b) S, c) Co, and d) Ni for the CoNi-LDH/PEDOT:PSS hybrid structure.

monolayers enables the reorientation of the polymer chain. It has been reported that the conformational change would favor the charge hopping and transport in the PEDOT chain.[36,37] XPS measurements were carried out to explore in more detail the interaction between LDH monolayers and PEDOT:PSS layer. The S2*p* core level spectrum of the pristine PEDOT:PSS shows two types of signature emission signals (pink line in Figure 3b). The S2*p* emission ranging from 166 to 171 eV enables a deconvolution of the feature into two spin–split doublets: the pair at 168.8 and 170.2 eV associated with S atom in neutral PSSH and the couple at 168.4 and 169.6 eV corresponding to the ionic PSS-Na^+.[38] The binding energies at 164.1 and 165.

4 eV are attributed to the spin–split components of S atom in PEDOT.[39] In the case of S2*p* spectrum for CoNi-LDH/PEDOT:PSS (blue line in Figure 3b), the intensity of PEDOT-derived feature enhances dramatically upon the hybridization. The PEDOT-to-PSS ratio calculated by the integral peak areas significantly increases from 0.314 to 1.12, implying the partial removal of PSS after the assembly. Moreover, the disappearance of PSSH component demonstrates that the ionic PSS-Na^+ is dominant in the interlayer gallery of LDH monolayers, consistent with the mechanism of electrostatic self-assembly.

Raman spectroscopy is a powerful technique for the study of conducting polymers, and so was employed to understand

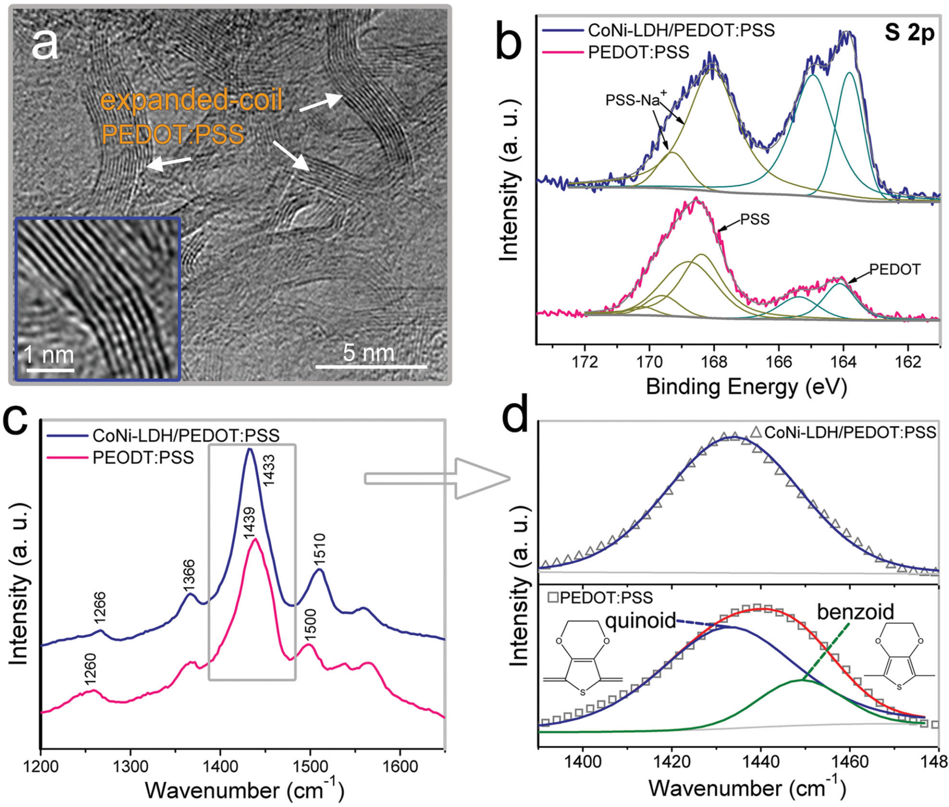

Figure 3. a) TEM image of PEDOT:PSS chains in the CoNi-LDH/PEDOT:PSS; b) XPS spectra and c) Raman spectra of CoNi-LDH/PEDOT:PSS and pristine PEDOT:PSS; d) corresponding deconvolution of the Raman spectra for CoNi-LDH/PEDOT:PSS and pristine PEDOT:PSS.

the hybridization at a molecular level. The Raman spectra of PEDOT:PSS and CoNi-LDH/PEDOT:PSS are shown in Figure 3c,d; typical peaks are identified in Table S1 and Figure S8 (Supporting Information). The most marked difference is observed in the region around the strongest band (1400–1470 cm^{-1}), corresponding to the symmetric C_{α}=C_{β} stretching mode of the PEDOT thiophene ring.[36] Two kinds of resonant structures of PEDOT, the benzoid and quinoid form, inherently determine the electronic property of PEDOT:PSS.[33,36,40] The benzoid (insulating or semiconducting) form possesses a π-electron localized structure; while the quinoid (conducting) form holds a delocalized state of π-electrons.[33,34] The band (centered at 1439 cm^{-1}) of pure PEDOT:PSS can be deconvoluted into two vibrations at 1447 and 1433 cm^{-1}, demonstrating the a mixture of both benzoid and quinoid resonant form (Figure 3d). In contrast, the CoNi-LDH/PEDOT:PSS hybrid exhibits a narrower and more symmetrical band, which is fit well by only the vibration at 1433 cm^{-1}. The disappearance of the shoulder peak at 1447 cm^{-1} reveals the influence of inorganic–organic hybridization on the resonant structure of PEDOT chains: the benzoid form transforms into the quinoid form after the assembly, and the conducting form (quinoid form) becomes dominant in the CoNi-LDH/PEDOT:PSS hybrid. However, this change cannot be detected in the physical mixture sample of CoNi-LDH and PEDOT:PSS (Figure S9, Supporting Information), verifying this specific interaction only occurs within the superlattice structure. The surface conductivity of CoNi-LDH/PEDOT:PSS thin film on glass substrate was measured via the four-point probe technique, giving a value of 125 S m^{-1}, much larger than that of pure PEDOT:PSS (30 S m^{-1}) and CoNi-LDH+PEDOT:PSS physical mixture (46 S m^{-1}). As a result, an improved charge-carrier mobility is achieved along the *ab*-plane of the superlattice CoNi-LDH/PEDOT:PSS.

2.2. Electrochemical Performance of the CoNi-LDH/PEDOT:PSS Hybrid Electrode

The electrochemical behavior of CoNi-LDH/PEDOT:PSS hybrid electrode was studied by cyclic voltammetry (CV), galvanostatic charge–discharge (CD), and electrochemical impedance spectroscopy (EIS) tests using a three-electrode system. **Figure 4**a shows typical CV curves of the CoNi-LDH/PEDOT:PSS electrode over the scan range 20–200 mV s^{-1}. Two pairs of well-defined redox peaks during the anodic and cathodic sweeps are explicitly observed, related to the electron-transfer pseudocapacitive processes of Co^{2+}/Co^{3+} (0.29 and 0.20 V) and Ni^{2+}/Ni^{3+} (0.36 and 0.26 V) with the assistance of OH^- given below.

$$Co(OH)_2 + OH^- \leftrightarrow CoOOH + H_2O + e^- \quad (1)$$

$$Ni(OH)_2 + OH^- \leftrightarrow NiOOH + H_2O + e^- \quad (2)$$

With an increase of the scan rate, the redox current peaks increase linearly, suggesting a surface-controlled

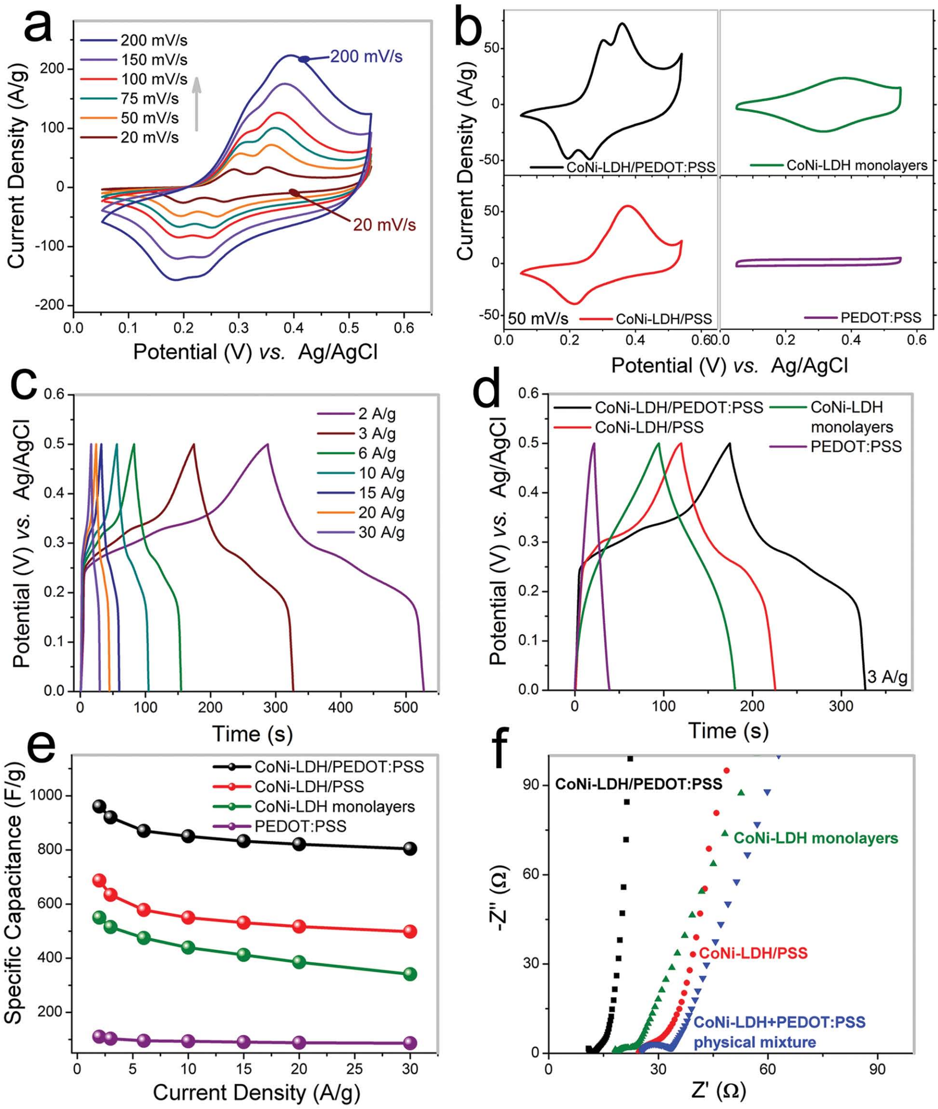

Figure 4. Electrochemical performances: a) CV curves of CoNi-LDH/PEDOT:PSS at various scan rates; b) CV curves of CoNi-LDH/PEDOT:PSS, CoNi-LDH/PSS, CoNi-LDH monolayers and PEDOT:PSS; c) CD curves of CoNi-LDH/PEDOT:PSS at various current densities; d) CD curves of CoNi-LDH/PEDOT:PSS, CoNi-LDH/PSS, CoNi-LDH monolayers and PEDOT:PSS; e) specific capacitance as a function of current density; f) Nyquist plots of CoNi-LDH/PEDOT:PSS, CoNi-LDH/PSS, CoNi-LDH monolayers and CoNi-LDH+PEDOT:PSS physical mixture.

electrochemical process and good pseudocapacitive behavior. Inspite of a slight shift of redox peaks, the CV shape shows small distortions even at a scan rate of 200 mV s^{-1}.

The CV curves of CoNi-LDH/PEDOT:PSS, CoNi-LDH/PSS, CoNi-LDH monolayers, and PEDOT:PSS electrode are shown in Figure 4b. Both the CoNi-LDH monolayers and CoNi-LDH/PSS display a pair of broad peaks, arising from bimetallic redox reactions of the LDH host layer.[29,42] The as-obtained CoNi-LDH/PEDOT:PSS possesses an improved capacitive behavior compared with CoNi-LDH/PSS, CoNi-LDH monolayers, and PEDOT:PSS. Specifically, the great enhancement of peak current and the integrated area is indicative of its high capacitance, which can be ascribed to the superlattice hybrid structure. In addition, the CoNi-LDH/PEDOT:PSS displays both enhanced currents and depressed peak voltage difference, in comparison with the CoNi-LDH+PEDOT:PSS physical mixture (Figure S10, Supporting Information), further demonstrating the merit of the molecular-scale architecture. The electrochemical behavior of CoNi-LDH/PEDOT:PSS samples with various Co/Ni ratios were also investigated (Figure S11, Supporting Information). The integrated area expands with boosted gravimetric current density as Co/Ni ratio decreases (3:1 to 2:1), while a dramatic decay in current density is observed upon further decreasing the Co/Ni ratio. The sample of Co_2Ni_1-LDH/PEDOT:PSS shows the optimum electrochemical performance.

The CoNi-LDH/PEDOT:PSS electrode also exhibits distinct galvanostatic CD behavior, as shown in Figure 4c. Unlike the isosceles triangle characteristic of electronic double-layer capacitor, the discharge curves of CoNi-LDH/PEDOT:PSS electrode show a typical pseudocapacitive behavior, which agrees very well with CV results. The observed symmetrical response implies the high columbic efficiency at all the current densities.

Compared with other samples, the CoNi-LDH/PEDOT:PSS electrode exhibits a much higher specific capacitance (920 F g^{-1}) and longer discharge time at the same current density of 3 A g^{-1} (Figure 4d), indicating the redox active LDH monolayers and the conducting polymer synergistically improve the capacitive performance. Figure 4e further illustrates the relationship between the specific capacitance and current density on the basis of the discharge curve. Within the whole current density range, the CoNi-LDH/PEDOT:PSS electrode produces the highest specific capacitance. At a high current density of 30 A g^{-1}, 83.7% of the capacitance (from 960 to 804 F g^{-1}) is retained for the CoNi-LDH/PEDOT:PSS, surpassing the other comparison electrodes as well as recently reported carbon-assisted Co–Ni nanostructured electrodes (e.g., hydroxide and sulfide).[41–44]

To gain further insight into the advantages of the molecular-scale hybrid structure, we employed EIS measurements (Figure 4f). The Nyquist plots of CoNi-LDH monolayers and CoNi-LDH+PEDOT:PSS physical mixture show a straight ≈45° sloped tail at low-frequency region, representative of the ion diffusion characteristic within the pores of the electrode.[9,45] For the CoNi-LDH/PSS electrode, an increased slope of the low-frequency tail is observed, which can be attributed to the additional ion-buffering reservoir provided by the extended interlayer space between LDH monolayers (1.00 nm). In the case of CoNi-LDH/PEDOT:PSS, further enlargement of the interlayer distance by PEDOT:PSS (1.40 nm) leads to a nearly vertical line as expected, as a result of the facilitated ion penetration and diffusion. In the high-frequency region, the real axis intercept is the equivalent series resistance (ESR), and the diameter of arc is indicative of the charge-transfer resistance (R_{ct}) in the electrode.[6,46] The CoNi-LDH/PEDOT:PSS shows both less ESR and R_{ct} than the other comparison electrodes, in-line with the conductivity enhancement by virtue of the PEDOT:PSS confined in the LDH interlayer.

The significantly improved capacitive behavior of the CoNi-LDH/PEDOT:PSS hybrid can be attributed to the architecture of the molecular-scale heterostructure. The LDH interlayer gallery provides a confined microenvironment for the accommodation of PEDOT:PSS with optimized spatial arrangement and doping level, which is reflected by the transformation of resonant structure (benzoid form to quinoid form). The ultrathin CoNi-LDH monolayers, acting as 2D polycations with an electrophilic function, are supposed to draw the delocalized electrons from PEDOT. The π backbone of PEDOT experiences an effective p-type doping process (Figure S12, Supporting Information), giving rise to a conducting state to offer in-plane charge-carrier highways.[33,34] On the contrary, the extended interlayer distance (1.40 nm) enables an open network for the electrolyte (e.g., OH$^-$) collection and diffusion throughout the ordered hybrid material. Our results demonstrate the molecular-scale hybridization with alternating inorganic redoxable layer and organic conducting layer boosts charge-carrier and ion transport simultaneously, guaranteeing a sufficient utilization of active sites during the electrochemical process.

2.3. In-Plane SC Device Based on the CoNi-LDH/PEDOT:PSS Thin Film

In order to integrate the as-synthesized CoNi-LDH/PEDOT:PSS hybrid material into large-scale compact thin films, we adopt a vacuum-filtration approach through a nitrocellulose membrane and then transfer to various target substrates (Figure S13, Supporting Information). The resulting CoNi-LDH/PEDOT:PSS thin films are uniform, translucent and mechanically flexible (**Figures 5**a and S13, Supporting Information). The *c*-oriented layered structure is preserved with tunable thickness, as observed in the cross-sectional SEM image (Figure S14, Supporting Information). To meet the demands of high-performance energy storage, it is essential to increase the energy density of SCs, without sacrificing the device power density and cycle life. To demonstrate its application in the miniaturized energy storage, we fabricated an all-solid-state SC based on the CoNi-LDH/PEDOT:PSS film (positive) and reduced grapheme oxide (rGO) film (negative) with an in-plane interdigital design (Figure 5b). Compared with a symmetric design, the asymmetric SC configuration takes advantage of largely increased device operating voltage and hence significantly enhanced energy density.[5,7] The rGO-based film exhibits good electrical and mechanical properties, which meet the prerequisites for thin-film electronic devices.[29,47] Typically, an array of parallel thin-film strips was obtained as the working electrodes on a polyethylene terephthalate (PET) substrate using PVA/KOH electrolyte without any binder or packaging material. The mass ratio of the CoNi-LDH/PEDOT:PSS to rGO was controlled ≈0.48 based on the specific capacitance and potential range (Figure S15, Supporting Information).[7] The microscopic planar configuration provides the horizontal transport pathway for electrolyte ions, superlative for the CoNi-LDH/PEDOT:PSS hybrid material with well-defined 2D arrangement.[47]

Within a large voltage window of 1.2 V, CV curves of the SC device were acquired at various scan rates (Figure 5c). Unlike the three-electrode electrochemical feature of CoNi-LDH/PEDOT:PSS electrode, the resulting SC device displays a quasi-rectangular CV geometry, revealing a nearly ideal capacitive behavior. The pronounced broad peaks at 1.0 (oxidation peak) and 0.7 V (reduction peak) arise from the redox reactions of LDH monolayers with the assistance of neighboring conductive PEDOT:PSS. Taking advantage of the efficient in-plane charge transport, the peak voltage difference remains constant upon increasing scan rate up to 400 mV s^{-1}. As illustrated in Figure 5d, all CD curves show a very rapid current response on the voltage reversal at each end potential. Accordingly, the as-fabricated in-plane SC based on the CoNi-LDH/PEDOT:PSS film and rGO film yields specific capacitances of 264, 251, 243, 238, and 230 F g^{-1} at current densities of 2, 4, 8, 12, and 20 A g^{-1}, respectively. In addition, compared with the traditional stacked-type geometry, the in-plane design allows for a full utilization of electrochemically active species, achieving largely enhanced energy storage performances (Figures S16,S17, Supporting Information). In the current density range investigated, the in-plane SC yields substantially higher capacitances than the stacked SC. At 20 A g^{-1}, the rate capability of stacked SC drops to 49% while the in-plane SC remains 82%.

The energy and power density, calculated from CD curves and plotted on the Ragone diagram (Figure 5e), further evaluate the energy efficiency of this SC device. Impressively, a high energy density of 46.1 Wh kg^{-1} at a power density of 11.9 kW kg^{-1} is delivered, which outperforms previously reported thin-film SC systems such as MnO$_2$/rGO,[17] GO-doped in gel,[12] aligned

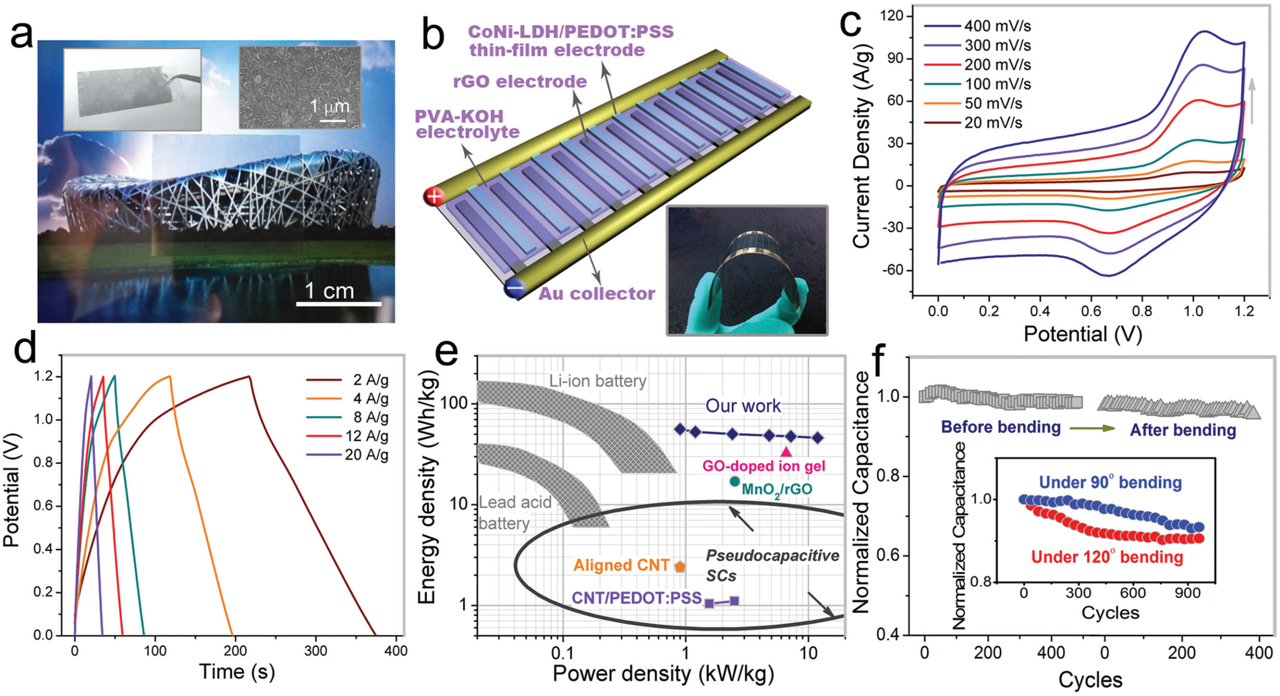

Figure 5. a) Optical photographs of the CoNi-LDH/PEDOT:PSS thin film on a transparent and flexible polyethylene terephthalate (PET) substrate (inset: corresponding SEM image); b) schematic illustration of the flexible in-plane SC device based on interdigital CoNi-LDH/PEDOT:PSS thin film and rGO thin film (inset: demonstration of the flexibility); c) CV curves of the device at various scan rates; d) CD curves of the device at various current densities; e) Ragone plots of the in-plane SC device; f) cycling performance at a current density of 12 A g^{-1} before and after bending to 90° for 400 times (inset: capacitance retention under 90° and 120° bending angles during 1000 cycles).

CNT,[8] and CNT/PEDOT:PSS.[45] The maximum energy density of 56.2 Wh kg^{-1} is achieved in this work, which is two times higher than that of lead acid batteries (25–35 Wh kg^{-1}) and nearly one order of magnitude higher than those of commercial activated carbon-based SCs (4–5 Wh kg^{-1}).[48,49] The SC device was further subjected to mechanical bending and cycling tests. After bending 400 times at 90°, the device retains more than 96% of its initial capacitance at 12 A g^{-1} (Figure 5f). Under bending angles of 90° and 120°, 93% and 90% of its initial capacitance are retained after 1000 cycles (inset of Figure 5f), demonstrating the high flexibility and stability desirable for thin-film electronics. SEM analysis was further performed on the used film electrode after 1000 cycles under 90° bending (Figure S18, Supporting Information). No obvious change is observed both in the film surface and film-substrate interface morphology, indicating excellent adherence of electrochemically active material to the substrate. The coulombic efficiency increases gradually from 68.1% for the first cycle to 83.3% for the 500th cycle (Figure S19, Supporting Information), as a result of the self-activation process.[2] In addition, the rather low IR drop (0.028 V) observed in Figure S19 (Supporting Information) implies a small intrinsic series resistance inside the SC device. To further demonstrate the application of this thin-film SC for electronic and optoelectronic devices, a fully charged thin-film SC was used to power an UV photodetector based on TiO$_2$ nanowire arrays grown on a fluorine-doped tin oxide (FTO) glass (**Figure 6**a). Driven by the thin-film SC, the photodetector delivers a steady and prompt response upon UV light irradiation (254 nm), as shown in Figure 6b. Further improvements in the patterned configuration (e.g., the size of electrode, the space between electrodes) and the conductivity of electrolytes (e.g., the addition of ionic liquids), are expected to allow higher power and energy characteristics for this thin-film SC.

3. Conclusion

In summary, a facile assembly of PEDOT:PSS with CoNi-LDH monolayers was developed for SC applications. Two counterpart building blocks were proved to sandwich each other in alternating sequence on a molecular scale, as in the experimental observation. The existence of LDH monolayer leads to a resonant and conformational change of PEDOT chains, allowing the high charge-carrier mobility. In this homogeneous hybrid configuration, CoNi-LDH monolayers play the role of

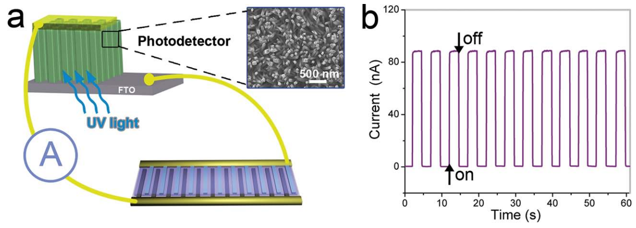

Figure 6. a) Schematic illustration of the UV photodetector based on the TiO$_2$ nanowire array driven by an in-plane SC (inset: SEM image of the TiO$_2$ nanowire array); b) current response of the photodetector upon intermittent UV irradiation.

electrochemically active species while sandwiched PEDOT:PSS layers enable effective charge transport and electrode integrity, thus endowing the hybrid electrode with high capacity, high rate-capability and excellent cycling stability. An in-plane SC device with 2D transport pathways for electrolyte ions was further fabricated, which is rather suitable for the *c*-oriented layered arrangement of hybrid structure. The combination of CoNi-LDH/PEDOT:PSS thin film and a compatible planar design leads to superior energy storage performances: high energy and power density, satisfactory cycling stability and flexibility. From a practical standpoint, such a 2D molecular-scale strategy can be easily adapted to various structural designs for energy storage and conversion devices such as lithium-ion batteries, water splitting cells, and photodetectors.

4. Experimental Section

Preparation of LDH Precursors: Briefly, 5.0×10^{-3} M of $CoCl_2 \cdot 6H_2O$, 2.5×10^{-3} M of $NiCl_2 \cdot 6H_2O$ (a total concentration of 7.5×10^{-3} M) and 45×10^{-3} M of hexamethylenetetramine (HMT) were dissolved in 1000 mL three-neck flask with deionized Milli-Q water. The resulting solution was refluxed for 6 h under nitrogen protection and continuous stirring. The pink brucite precipitate (CoNi-hydroxide) was obtained by filtration, washed with deionized water and anhydrous ethanol in turn, and dried at room temperature. Subsequently, the CoNi-hydroxide phase (0.186 g) was dispersed in 100 mL of anhydrous acetonitrile (99.8%) containing 7.0 mmol of bromine. The mixture was sealed in an airtight capped flask and stirred for 24 h. The dark brown product, identified as Br^- intercalated CoNi-LDH phase, was collected by filtration and washed thoroughly with anhydrous ethanol. To prepare the nitrate intercalated CoNi-LDH, as-prepared 0.25 g CoNi-Br^--LDH powder was further added into a flask containing 0.3 mol of $NaNO_3$ into 200 mL of ethanol/water binary liquid (1:1, v/v). The flask was mechanically shaken at room temperature in nitrogen atmosphere for 48 h. The product was filtered, washed with anhydrous ethanol, and air-dried. The exfoliation was performed as follows: a 0.05 g of CoNi-NO_3^--LDH was dispersed in 100 mL of formamide in a flask sealed in nitrogen atmosphere, and then agitated in a mechanical shaker for 60 h, giving a colloidal suspension. The resulting translucent colloidal solution was further centrifugated to remove possible unexfoliated LDH particles.

Self-Assembly of the CoNi-LDH Monolayers and PEDOT:PSS: Based on the calculation of charge density of both LDH and PEDOT:PSS, a volume ratio of 32 between pristine CoNi-LDH monolayers and PEDOT:PSS solution was determined to meet the charge matching hypothesis. First, PEDOT:PSS suspension (1.56 mL) was diluted in formamide (15 mL) under constant stirring, followed by pouring into a colloidal solution of CoNi-LDH monolayers (50 mL). After stirring for 12 h accompanied in nitrogen atmosphere, the dark precipitate was centrifuged at 9000 rpm, and washed by deionized Milli-Q water. Finally, the obtained CoNi-LDH/PEDOT:PSS sample was preserved in water.

Fabrication of the CoNi-LDH/PEDOT:PSS Thin film and In-Plane SC Device: The SC device (area: 2 cm × 6 cm) was fabricated by a mechanical shaping process modified from the previously reported method.[17,46] The CoNi-LDH/PEDOT:PSS thin film was prepared by filtering the CoNi-LDH/PEDOT:PSS suspension through a nitrocellulose membrane (0.22 μm in pore size). The CoNi-LDH/PEDOT:PSS thin film obtained by vacuum filtration was rolled with a glass rod onto various substrates, e.g., flexible polyethylene terephthalate (PET) and rigid glass, followed by tightly pressing for 24 h and peeling off the membrane. A series of blades as the mold were stacked side by side accurately for shaping slim strips of the CoNi-LDH/PEDOT:PSS thin film (the positive electrodes for the SC). For the negative electrodes, the rGO film was fabricated by the same method. The mass of the thin films can be facilely controlled by changing the volume of CoNi-LDH/PEDOT:PSS or rGO suspension in the vacuum-filtration step. The mass loading of electrode was further confirmed by the mass difference between the as-prepared electrode and blank substrate. Two columns of Au charge collectors were deposited on the two ends of the substrate for the integration of the primary individual units into a typical in-planar SC device. The compact in-plane SC device was finally established after coated with solid-state electrolyte of PVA/KOH onto the CoNi-LDH/PEDOT:PSS and rGO strip-shaped electrodes.

Fabrication of the UV Photodetector: Vertical TiO_2 nanowire arrays were grown on FTO substrates by the reported hydrothermal method.[50] The UV detector was then prepared by coating the conducting Ag paste pad on top of the TiO_2 nanorod arrays. The backside illumination was adopted and the illuminated area under UV light (20 W) was ≈6 cm^2.

Material Characterization: The sample morphology was investigated using a scanning electron microscope (SEM; Zeiss SUPRA 55) with an accelerating voltage of 20 kV, combined with energy dispersive X-ray spectroscopy (EDS). The CoNi-LDH/PEDOT:PSS samples were embedded in resin followed by aging at 60 °C for 48 h and sectioned by ultramicrotome for cross-sectional TEM studies. TEM images were recorded with a JEOL JEM-3010. High-resolution TEM (HRTEM) and high-angle annular dark-field scanning TEM (HAADF-STEM) images were collected on an FEI Tecnai G2 F20 S-Twin working at 200 kV. The relative energy-dispersive X-ray spectrometry (EDS) elemental mapping and line scan in the STEM were operated with a probe focused to 0.2 nm and camera length of 20 cm. X-ray diffraction (XRD) patterns were recorded by a Rigaku XRD-6000 diffractometer, using Cu–Kα radiation (0.15418 nm) at 40 kV, 30 mA. X-ray photoelectron spectroscopy (XPS) measurements were performed using an ESCALAB 250 instrument (Thermo Electron) with Al Kα radiation. Raman measurements were carried out with 633 nm of excitation by using a confocal Raman microspectrometer (Renishaw, inVia-Reflex, 633 nm). A μAutolab II (Metrohm-Autolab, Netherlands) was employed for all the electrochemical measurements. For the three-electrode configuration, a silver/silver chloride (Ag/AgCl) electrode and a platinum plate serve as the reference and counter electrode, respectively. The CoNi-LDH/PEDOT:PSS thin film was transferred onto indium tin oxide (ITO) substrates as the working electrode in 1 M KOH aqueous solution. The EIS measurement was performed by applying an AC voltage with 5 mV amplitude in a frequency range 0.01–100 kHz. The specific capacitance was calculated from the charge-discharge curves based on the following equation

$$C_s = \frac{I \times \Delta t}{m \times \Delta V} \tag{3}$$

where C_s (F g^{-1}) is the specific capacitance; I (A) refers to the discharge current; ΔV (V) represents the potential change within the discharge time Δt (s), and m (g) corresponds to the total weight of the electrochemically active material. Energy density and power density of the SC device were calculated using the following equations

$$C = \frac{I \times \Delta t}{M \times \Delta V} \tag{4}$$

$$E = \frac{1}{2} \times C \times (\Delta V)^2 \tag{5}$$

$$P = \frac{E}{\Delta t} \tag{6}$$

where C (F g^{-1}) is the capacitance of the SC device; I (A) represents the discharge current; ΔV (V) refers to the potential change within the discharge time Δt (s); M (g) is the mass loading of electrode; E (Wh kg^{-1}) and P (kW/kg^{-1}) correspond to the energy density and power density, respectively.

Supporting Information

Supporting Information is available from the Wiley Online Library or from the author.

Acknowledgements

This work was supported by the 973 Program (Grant No.: 2011CBA00504), the National Natural Science Foundation of China (NSFC), the Scientific Funds from Beijing Municipal Commission of Education (Grant No. 20111001002) and the Fundamental Research Funds for the Central Universities (YS1406). M. W. particularly appreciates the financial aid from the China National Funds for Distinguished Young Scientists of the NSFC. K.T. acknowledges support by a Marie Curie Intra European Fellowship within the 7th European Community Framework Programme.

Received: January 31, 2015
Revised: February 24, 2015

---

[1] D. R. Rolison, R. W. Long, J. C. Lytle, A. E. Fischer, C. P. Rhodes, T. M. McEvoy, M. E. Bourga, A. M. Lubers, *Chem. Soc. Rev.* **2009**, *38*, 226.
[2] L. Yuan, B. Yao, B. Hu, K. Kuo, W. Chen, J. Zhou, *Energy Environ. Sci.* **2013**, *6*, 470.
[3] H. Nishide, K. Oyaizu, *Science* **2008**, *319*, 737.
[4] J. H. Pikul, H. G. Zhang, J. Cho, P. V. Braun, W. P. King, *Nat. Commun.* **2013**, *4*, 1732.
[5] M. F. El-Kady, R. B. Kaner, *Nat. Commun.* **2013**, *4*, 1475.
[6] W. W. Liu, Y. Q. Feng, X. B. Yan, J. T. Chen, Q. J. Xue, *Adv. Funct. Mater.* **2013**, *23*, 4111.
[7] J. Chang, M. Jin, F. Yao, T. H. Kim, V. T. Le, H. Yue, F. Gunes, B. Li, A. Ghosh, S. Xie, Y. H. Lee, *Adv. Funct. Mater.* **2013**, *23*, 5074.
[8] T. Chen, H. Peng, M. Durstock, L. Dai, *Sci. Rep.* **2014**, *4*, 3612.
[9] Z. Niu, H. Dong, B. Zhu, J. Li, H. H. Hng, W. Zhou, X. Chen, S. Xie, *Adv. Mater.* **2013**, *25*, 1058.
[10] X. Xiao, T. Q. Li, Z. H. Peng, H. Y. Jin, Q. Z. Zhong, Q. Y. Hu, Q. P. Luo, C. F. Zhang, L. Gong, J. Chen, Y. Gogotsi, J. Zhou, *Nano Energy* **2014**, *6*, 1.
[11] D. Pech, M. Brunet, H. Durou, P. Huang, V. Mochalin, Y. Gogotsi, P. L. Taberna, P. Simon, *Nat. Nanotechnol.* **2010**, *5*, 651.
[12] X. Yang, F. Zhang, L. Zhang, T. Zhang, Y. Huang, Y. Chen, *Adv. Funct. Mater.* **2013**, *23*, 3353.
[13] J. Ji, L. L. Zhang, H. Ji, Y. Li, X. Zhao, X. Bai, X. Fan, F. Zhang, R. S. Ruoff, *ACS Nano* **2013**, *7*, 6237.
[14] X. Xiao, X. Peng, H. Jin, T. Li, C. Zhang, B. Gao, B. Hu, K. Huo, J. Zhou, *Adv. Mater.* **2013**, *25*, 5091.
[15] C. Wu, X. Lu, L. Peng, K. Xu, X. Peng, J. Huang, G. Yu, Y. Xie, *Nat. Commun.* **2013**, *4*, 1732.
[16] C. Zhou, Y. Zhang, Y. Li, J. Liu, *Nano Lett.* **2013**, *13*, 2078.
[17] L. Peng, X. Peng, B. Liu, C. Wu, Y. Xie, G. Yu, *Nano Lett.* **2013**, *13*, 2151.
[18] X. Xiao, T. Ding, L. Yuan, Y. Shen, Q. Zhong, X. Zhang, Y. Cao, B. Hu, T. Zhai, L. Gong, J. Chen, Y. Tong, J. Zhou, Z. L. Wang, *Adv. Energy Mater.* **2012**, *2*, 1328.
[19] R. Liu, S. B. Lee, *J. Am. Chem. Soc.* **2008**, *130*, 2942.
[20] S. Hu, X. Wang, *Chem. Soc. Rev.* **2013**, *42*, 5577.
[21] R. Ma, T. Sasaki, *Adv. Mater.* **2010**, *22*, 5082.
[22] A. M. Fogg, V. M. Green, H. G. Harvey, D. O'Hare, *Adv. Mater.* **1999**, *11*, 1466.
[23] M. Q. Zhao, Q. Zhang, J. Q. Huang, F. Wei, *Adv. Funct. Mater.* **2012**, *22*, 675.
[24] C. G. Silva, Y. Bouizi, V. Fornés, H. García, *J. Am. Chem. Soc.* **2009**, *131*, 13833.
[25] F. Leroux, J. P. Besse, *Chem. Mater.* **2001**, *13*, 3507.
[26] L. Li, R. Ma, Y. Ebina, K. Fukuda, K. Takada, T. Sasaki, *J. Am. Chem. Soc.* **2007**, *129*, 8000.
[27] Q. Wang, D. O'Hare, *Chem. Rev.* **2012**, *112*, 4124.
[28] E. Coronado, C. Martí-Gastaldo, E. Navarro-Moratalla, A. Ribera, S. J. Blundell, P. J. Baker, *Nat. Chem.* **2010**, *2*, 1031.
[29] R. Ma, X. Liu, J. Liang, Y. Bando, T. Sasaki, *Adv. Mater.* **2014**, *26*, 4173.
[30] F. Song, X. Hu, *Nat. Commun.* **2014**, *5*, 4477.
[31] F. Leroux, C. T. Guého, *J. Mater. Chem.* **2005**, *15*, 3628.
[32] L. Nyholm, G. Nyström, A. Mihranyan, M. Strømme, *Adv. Mater.* **2011**, *23*, 3751.
[33] J. L. Brédas, B. Thémans, J. G. Fripiat, J. M. André, *Phys. Rev. B* **1984**, *29*, 6761.
[34] A. G. MacDiarmid, *Angew. Chem. Int. Ed.* **2001**, *40*, 2581.
[35] S. Biswas, L. T. Drzal, *Chem. Mater.* **2010**, *22*, 5667.
[36] J. Ouyang, C. W. Chu, F. C. Chen, Q. Xu, Y. Yang, *Adv. Funct. Mater.* **2005**, *15*, 203.
[37] D. Alemu, H. Y. Wei, K. C. Ho, C. W. Chu, *Energy Environ. Sci.* **2012**, *5*, 9662.
[38] T. P. Nguyen, S. A. De Vos, *Appl. Surf. Sci.* **2004**, *221*, 330.
[39] C. H. L. Weijtens, V. Van Elsbergen, M. M. De Kok, S. H. P. M. De Winter, *Org. Electron.* **2005**, *6*, 97.
[40] Y. S. Hsiao, W. T. Whang, C. P. Chen, Y. C. Chen, *J. Mater. Chem.* **2008**, *18*, 5948.
[41] D. Zhou, X. Su, M. Boese, R. Wang, H. Zhang, *Nano Energy* **2014**, *5*, 52.
[42] J. Xiao, L. Wan, S. Yang, F. Xiao, S. Wang, *Nano Lett.* **2014**, *14*, 831.
[43] H. Chen, L. Hu, M. Chen, Y. Yan, L. Wu, *Adv. Funct. Mater.* **2014**, *24*, 934.
[44] C. Yuan, J. Li, L. Hou, X. Zhang, L. Shen, X. W. Lou, *Adv. Funct. Mater.* **2012**, *22*, 4592.
[45] D. Antiohos, G. Folks, P. Sherrell, S. Ashraf, G. G. Wallace, P. Aitchison, A. T. Harris, J. Chen, A. I. Minett, *J. Mater. Chem.* **2011**, *21*, 15987.
[46] Z. Weng, Y. Su, D. W. Wang, F. Li, J. Du, H. M. Cheng, *Adv. Energy Mater.* **2011**, *1*, 917.
[47] J. J. Yoo, K. Balakrishnan, J. Huang, V. Meunier, B. G. Sumpter, A. Srivastava, M. Conway, A. L. M. Reddy, J. Yu, R. Vajtai, P. M. Ajayan, *Nano Lett.* **2011**, *11*, 1423.
[48] A. Burke, *Electrochim. Acta* **2007**, *53*, 1083.
[49] Y. Xu, Z. Lin, X. Zhong, X. Huang, N. O. Weiss, Y. Huang, X. Duan, *Nat. Commun.* **2014**, *5*, 4554.
[50] B. Liu, E. S. Aydil, *J. Am. Chem. Soc.* **2009**, *131*, 3985.